24th COBEM - 2017

24th ABCM International Congress of Mechanical Engineering
December 3-8, 2017, Curitiba, PR, Brazil

COBEM-2017-0684
ANALYSIS OF MIXED-MODE STRESS INTENSITY FACTORS USING DIGITAL IMAGE CORRELATION DISPLACEMENT FIELDS

Jorge Guillermo Díaz Rodríguez
jorgeguillermo12@ustabuca.edu.co
División de Ingenierías. Universidad Santo Tomás. Carrera 18#9-27. Bucaramanga, Colombia
Giancarlo Luis Gómez Gonzáles
gonzalesglg@aaa.puc-rio.br
Julián Andrés Ortiz González
julian@aluno.puc-rio.br
José Luiz de França Freire
jlfreire@puc-rio.br
DEM PUC-Rio, Rua Marquês de São Vicente, 225, Gávea CEP: 22451-000 - Rio de Janeiro, Brasil

Abstract. *This paper presents two experimental approaches for determining the mode I and mode II stress intensity factors (SIFs) of a crack initiated and propagated by cyclic loading. The first measures the crack opening displacement (COD) and then evaluates SIFs from the first term of the Westergaard displacement function by using the least-squares method. The second determines coefficients of generalized Westergaard function from the full-field displacement data around the crack by an over-deterministic linear Least Square scheme. From the estimated coefficients, the SIF values can be determined. Both approaches use the displacement field measured by the Digital Image Correlation (DIC) technique. The fatigue test was performed on a modified compact tension C(T) specimen made out of low carbon steel, in which a hole was machined to curve the crack propagation path, inducing the I/II mixed mode.*

Keywords: *mixed mode fracture, DIC, crack propagation, LEFM.*

1. INTRODUCTION

The determination of mode I stress intensity factors (SIFs) from experimental full field displacement data using digital image correlation (DIC) was addressed for the first time in 1982 at the University of South Carolina (Peters and Ranson 1982). Later in 1983 (Sutton et al. 1983), a paper described a method to estimate deformation from an stretched photographed sample and another one (Peters et al. 1983) described how to compute rigid body displacements. With the advance of digital cameras, enhanced computing capacity and optimized algorithms, more accurate SIF solutions have been achieved. In 2006, Roux and Hild (Roux and Hild 2006) measured SIFs using eight complex-number fitting curves, each one for a different parameter, on their own DIC code. Yoneyama et. al. (Yoneyama, Morimoto, and Takashi 2006) estimated SIF, crack tip location (CTL) and higher-order terms in the William´s expansion of displacement fields using the least square method. In the same year (Ju, Liu, and Liu 2006) used digital photographs to record strategically-marked-points displacements, fit them to the Westergaard's stress function and solved the over deterministic matrix by the least squares method. Lopez-Crespo et. al (Lopez-Crespo et al. 2008) calculated SIF by fitting DIC measurements to the Muskhelishvili stress function, and attempted to locate the CTL using image processing techniques. On year later, Yates et. al. (Yates et al. 2009) used DIC to measure SIF, T-stress and the crack tip opening angle (CTOA) from displacement fields by fitting data to the Westergaard's stress function. In 2012 Zhang and He (Zhang and He 2012) used DIC to compute SIF, T-stress, rigid body motion, and rotation by fitting displacement fields under mixed loading conditions to the Westergaard's stress function. They used a refined grid to pinpoint more accurately the CTL by minimizing the error between the experimental displacements and the fitted displacements. More recently, Harilal et. al. (Harilal, Vyasarayani, and Ramji 2015) used a similar approach as Zhang and He, but they introduced crack tip coordinates as unknowns into the Williams solution. Gonzáles et. al. (Gonzáles et al. 2016), using an approach similar to Zhang, measured SIF mode I before and after overloads and warned about the careful interpretation of SIF results. Vormwald et. al. (Vormwald et al. 2017) measured SIF in three modes using the relative displacement of only two points. In all these methods, intrinsically it is assumed that the determined displacement field fit a predetermined linear elastic field and so they are limited to linear elastic fracture mechanics (LEFM) models.

Other approaches used to calculate SIF include Elasto-Plastic Fracture Mechanics parameters such as the J integral. Becker et. al (Becker et al. 2012) used the J integral approach. Assuming small scale yield, they did FEM simulation, exported displacement fields and calculated SIF using the elastic relation between SIF and J-integral. Then, following the same procedure for DIC data, they compared both values. The advantage of the J-integral approach is that the CTL does not have to be pinpointed accurately. Also, if the selected contour lies within the elastic part of the field, the non-linear area can be avoided. Yoneyama et. al (Yoneyama et al. 2014) evaluated J-integral using path and area formulations that included non-linear behavior by modeling the stress-strain behavior with a Ramberg-Osgood material model. On the other hand, Rethoré et. al. (Réthoré et al. 2005) used the interaction integral to calculate the SIF on a plate with a slanted crack. The interaction integral superposes two solutions assuming that one of them is known, the auxiliary field, the other one being calculated from the J-integral. Although this method is widely used in FEM codes, this approach still relies on the crack tip location (CTL) for the auxiliary displacement fields.

Cracks can deflect from the mode I preferential path due to multiaxial loads, environmental conditions, overloads or grain boundaries (Castro and Meggiolaro 2016). This problem was addressed in 2003 by Oliveira et. al. (De Oliveira Miranda et al. 2003), in which numerical simulations were performed to calculate the mixed mode SIF and to predict crack path direction. The simulation results were confirmed by actual fatigue experiments. In the present study, two experimental approaches using full field DIC displacement data for determining the mode I and mode II stress intensity factors (SIFs) were used to investigate the influence of mixed mode I and II SIFs on the crack path deflection. The first approach determines coefficients of the generalized Westergaard function from the full-field displacement data around the crack by the over-deterministic linear Least Square Method (LSM). From the estimated coefficients, the SIFs values can be determined. The second approach measures the crack opening displacement (COD), and then evaluates SIFs from the first term of the Westergaard displacement function by using the LSM. Both methodologies have been experimentally validated through crack growth on a modified compact tension C(T) specimen made of low carbon steel, in which a hole was machined to curve the crack propagation path, and therefore to calculate its associated SIFs, K_I and K_{II}.

2. METHODOLOGY

This section presents the relevant theoretical information needed along the paper.

2.1 Least-squares method using full-field displacement data

In the over-deterministic LSM approach, the Westergaard's stress function is used to determine the stress field ahead of the crack tip. This solution is written in the form of an infinite series expansion (Williams 1957), and describes the stress field around the crack tip region. For the displacement components, the asymptotic equations are defined by:

$$u = \sum_{n=1}^{\infty} \frac{A_n}{2G} r^{n/2} \left\{ \kappa \cos\frac{n}{2}\theta - \frac{n}{2}\cos\left(\frac{n}{2}-2\right)\theta + \left\{\frac{n}{2}+(-1)^n\right\}\cos\frac{n}{2}\theta \right\} - \sum_{n=1}^{\infty} \frac{B_n}{2G} r^{n/2} \left\{ \kappa \sin\frac{n}{2}\theta - \frac{n}{2}\sin\left(\frac{n}{2}-2\right)\theta + \left\{\frac{n}{2}-(-1)^n\right\}\sin\frac{n}{2}\theta \right\} \tag{1}$$

$$v = \sum_{n=1}^{\infty} \frac{A_n}{2G} r^{n/2} \left\{ \kappa \sin\frac{n}{2}\theta + \frac{n}{2}\sin\left(\frac{n}{2}-2\right)\theta - \left\{\frac{n}{2}+(-1)^n\right\}\sin\frac{n}{2}\theta \right\} - \sum_{n=1}^{\infty} \frac{B_n}{2G} r^{n/2} \left\{ -\kappa \cos\frac{n}{2}\theta - \frac{n}{2}\cos\left(\frac{n}{2}-2\right)\theta + \left\{\frac{n}{2}-(-1)^n\right\}\cos\frac{n}{2}\theta \right\} \tag{2}$$

Particularly, the first terms of the series A_1 and B_1 are related to the mode I and mode II SIFs as shown in Eqs. (3) and (4).

$$A_1 = \frac{K_I}{(2\pi)^{1/2}} \tag{3}$$

$$B_1 = \frac{K_{II}}{(2\pi)^{1/2}} \tag{4}$$

The displacements shown in Eqs. (1) and (2) are rewritten considering the possible rigid body motion (i.e. translation and rotation). When these terms are included, the crack tip displacement equations become:

$$u = \sum_{n=1}^{N} A_n f_{In}(r,\theta) - \sum_{n=1}^{N} B_n f_{IIn}(r,\theta) + T_x - Ry \tag{5}$$

$$v = \sum_{n=1}^{N} A_n g_{In}(r,\theta) - \sum_{n=1}^{N} B_n g_{IIn}(r,\theta) + T_y + Rx \tag{6}$$

where n is the number of terms of the series expansion of the displacement field, R is the rigid body rotation, and Tx and Ty are the components of the rigid body translation along the x and y directions, respectively. The terms f_I, f_{II}, g_I and g_{II} are functions in terms of the polar coordinates r and θ, with origin at the crack tip and angles being positive when referenced counter-clockwise from the crack extension direction as depicted in Figure 1.

Considering a set of m points collected from the region surrounding the crack tip, as shown in Figure 6, Eqs. (5) and (6) can be arrayed in the matrix form as:

$$[U] = [C] \cdot [\Delta] \tag{7}$$

where:

$$[U] = \begin{bmatrix} u_1 & \cdots & u_m & v_1 & \cdots & v_m \end{bmatrix}^T \tag{8}$$

$$[\Delta] = \begin{bmatrix} A_1 & \cdots & B_1 & \cdots & T_x & T_y & R \end{bmatrix}^T \tag{9}$$

$$[C] = \begin{bmatrix} f_{I1}(r_1,\theta_1) & \cdots & -f_{II1}(r_1,\theta_1) & \cdots & 1 & 0 & -y_1 \\ \vdots & \ddots & \vdots & \ddots & \vdots & \vdots & \vdots \\ f_{\mathrm{Im}}(r_M,\theta_M) & \cdots & -f_{II\,\mathrm{m}}(r_M,\theta_M) & \cdots & 1 & 0 & -y_m \\ g_{I1}(r_1,\theta_1) & \cdots & -g_{II1}(r_1,\theta_1) & \cdots & 0 & 1 & x_1 \\ \vdots & \ddots & \vdots & \ddots & \vdots & \vdots & \vdots \\ g_{\mathrm{Im}}(r_m,\theta_m) & \cdots & -g_{I\,\mathrm{Im}}(r_m,\theta_m) & \cdots & 0 & 1 & x_m \end{bmatrix} \tag{10}$$

Therefore, by using the least squares method (LSM) to solve Eq. (7), the unknown parameters are determined as:

$$[\Delta] = \left[[C]^T \cdot [C] \right]^{-1} \cdot [C]^T \cdot [U] \tag{11}$$

Herein, this method is referred as LSM.

2.2 Least-squares method using crack opening displacements

Figure 1 represents an infinite cracked isotropic and linear-elastic plate, where x and y are the Cartesian coordinates of an arbitrary point with respect to the CTL. The crack surface is in the negative x direction; u and v are the displacement in x and y directions, respectively; r and θ are the polar coordinates of the same arbitrary point.

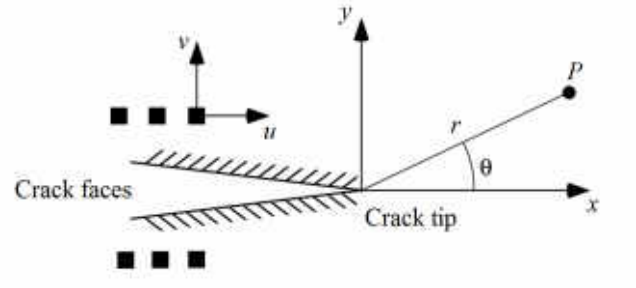

Figure 1. Crack tip coordinate system

Then, the crack opening displacements (COD) at the evaluation points in x and y directions are measured. From Eqs. (1) and (2), the COD in x and y directions, for an m-number of points can be arranged as follows:

$$CODx = \left[-f_{II1}(r_1,\theta_1) \quad -f_{II2}(r_2,\theta_2) \quad \ldots \quad -f_{IIm}(r_M,\theta_m)\right]\left[A_1 \quad A_2 \quad \ldots \quad A_m\right]^T \tag{12}$$

$$CODy = \left[g_{I1}(r_1,\theta_1) \quad g_{I2}(r_2,\theta_2) \quad \ldots \quad g_{Im}(r_m,\theta_m)\right]\left[B_1 \quad B_2 \quad \ldots \quad B_m\right]^T \tag{13}$$

Herein, this formulation is termed crack opening displacements with Least-squares method (COD-LSM).

3. DIGITAL IMAGE CORRELATION

Digital image correlation (Sutton, Orteu, and Schreier 2009) is currently the most popular and effective optical technique used in experimental mechanics to measure displacements and strains on the surface of stressed components. In essence, the DIC technique compares (or correlates) two digital images of the material surface acquired at different loading stages, one image that corresponds to the undeformed state (called the reference image), and the other that corresponds to the final or to a partial loading stage (deformed image). The image correlation process works by matching small square subsets of the reference image to locations in the deformed image as illustrated in Figure 2, by means of a cross correlation function. Once the location of all subsets in the deformed image is found, the displacement of each subset is determined, and from them the corresponding strain components can be obtained. For this technique to work adequately, the surface of the object must have a high-contrast granular morphology. Otherwise, the sample must be prepared beforehand by first painting its surface white and then applying over it a random pattern of small black dots (speckle pattern).

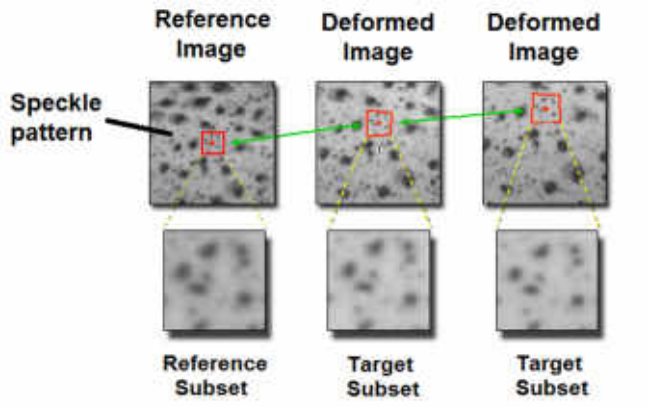

Figure 2 Principle of Digital Image Correlation [Correlated Solutions Inc].

4. MATERIALS AND MODELS

In this case, the mixed opening mode effect was created by drilling a hole in a Compact Tension C(T) specimen as shown in Figure 3a. The hole-modified C(T) specimen was made of a low carbon steel, with its lateral faces polished with sand paper No. 350 to minimize the presence of surface micro cracks and to better visualize the crack path. The material composition was obtained with a Thermo Scientific ® NITON XL5 X-Ray Fluorescence analyzer, giving the composition shown in Table 1.

Table 1. Chemical composition for modified C(T)sample.

Element	*Fe*	*Mn*	*Al*	*Si*	*S*	*P*	*Other*
%	98.04	0.61	0.42	0.125	0.02	0.014	0.75

A second chemical analysis was made using optical emission spectroscopy according to ASTM A751-2014a giving similar element composition and a 0.268% of Carbon content. After the tests, the sample was subjected to a Nital etching and observed under an optical microscope showing a Ferritic-Perlitic structure. This confirmed the material was indeed a low carbon steel.

The modified C(T) specimen was subjected to a cyclic axial load P, as shown in Figure 3b, using an INSTRON 8501 universal testing machine equipped with a 100 kN load cell. The crack was propagated, and about every 1 mm, the load frequency was lowered to allow image recording. Figure 3b shows a close-up of the experimental setup.

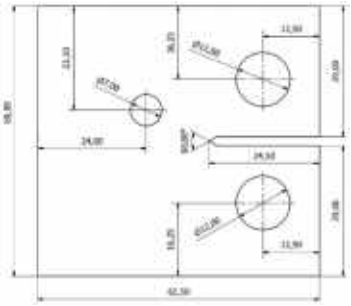

Figure 3(a) Holed CT specimen

(b) Testing set up

Although, due to the drilled hole, there were mixed-mode conditions, the tests were run under load control adjusting P to keep ΔK_I and K_{MAX} constant (ΔK=22 MPa-m$^{1/2}$ and R=0,1) using the standard ASTM E647-13 as a guide. The specimen´s polished face was primed with white paint and sprayed with random black speckles, according with DIC technique procedures. DIC photographs were taken when the optically-observed crack-growth increment was about 1 mm. Crack size measurements were indirectly measured and recorded with a strain gage bonded in the specimen´s back face, as shown in Figure 3b, and directly measured with an optical microscope following the horizontal component of the crack growth in the non-speckled side of the specimen. The loads P at the instant of each snapshot were recorded and stored along with the corresponding speckled images. Images were acquired with the 3D-VIC Snap ® software and processed later by the VIC-3D ® digital image correlation software, both from Correlated Solutions (Columbia, SC).

The 3D DIC system consists of two 5-MP cameras (Point Grey GRAS-50S5M) in a stereo configuration equipped with high magnification lenses. The DIC analysis was performed using a subset of 25 pixels, step of 6 pixels, and strain window size of 15. The spatial image resolution was of approximately 8.4 μm/pixel. An example of the DIC analysis is shown in Figures 4 and 5 where the displacement and strain fields surrounding the crack are plotted. Notice that the data points around the crack faces and very near to the crack tip were excluded from these analyses to avoid their high noise level. The high noise level refers to an inherent DIC characteristic. The correlation algorithm identifies the best-matching subsets between the reference and the deformed images. When in presence of a crack, the algorithm cannot distinguish crack sides, possibly matching gray intensities from opposite crack edges, therefore calculating unrealistic strains. Displacement field data was exported to be further processed in a Matlab® routine (Gonzáles et al. 2016) to calculate mixed mode SIFs values.

Figure 4a depicts *v*-component of the displacement field for a crack length of 4.1 mm at maximum applied load where only mode I is expected to have an influence on the crack. It can be seen that the displacements are perpendicular to the crack faces corresponding to the opening mode. Figure 4b depicts *u*-component of the displacement field at maximum applied load for a crack length of 11.85 mm. In this situation not only mode I but also mode II are expected. It is observed that the displacements are parallel to the crack faces and normal to the crack edge corresponding to the sliding mode or mode II. Moreover, Figures 5a and 5b (for total crack lengths of 4.1 and 11.85 mm respectively) depict the classical elastic butterfly strain field surrounding the crack tip at maximum applied load, where the highest strain values are found.

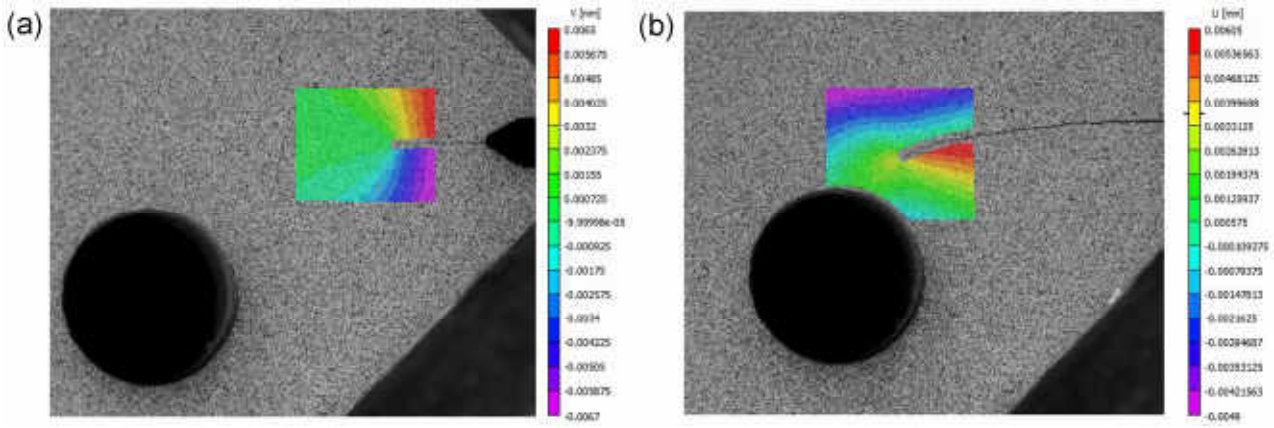

Figure 4. Exemplary results of measured displacement fields: a) Vertical displacement field for total crack length of 4.1 mm b) Horizontal displacement field for total crack length of 11.9 mm.

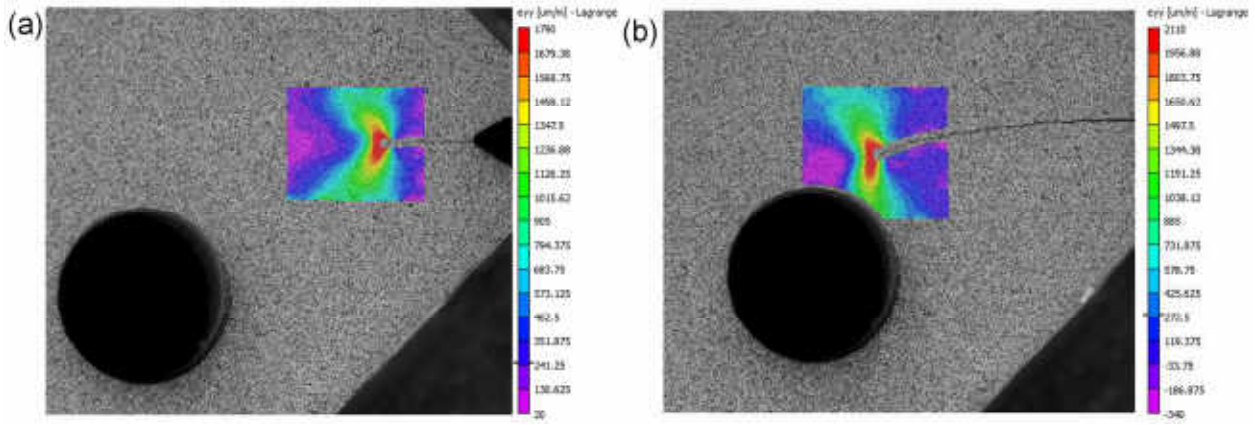

Figure 5. Exemplary results for strain distribution about the *y*-direction around the crack for: a) total crack length of 4.1 mm b) total crack length of 11.9 mm.

5. EXPERIMENTAL RESULTS

The C(T) specimen grew a crack initially horizontal which later curved due to the drilled hole. SIFs were calculated at total crack lengths of 4.1 mm, 6.3 mm, 8.2 mm, 10.2 and 11.9 mm. Figure 6a shows the CTL and the five points used to collect data from for SIF evaluation using the COD-LSM formulation. The symmetrical points were located at a distance of about 1 mm behind the crack tip and at 0.5 mm from the crack faces to avoid the higher noise level resulting from abrupt changes in displacement when the crack opens and closes during propagation. Figure 6b depicts the data points used in the over-determinist LSM formulation. In the same way, in order to avoid the intensively non-linear behavior around the crack tip and the crack faces, the data points inside this area were excluded from the DIC analyses. Moreover, to comply with Williams' equations, the displacement fields were aligned with the crack propagation angle.

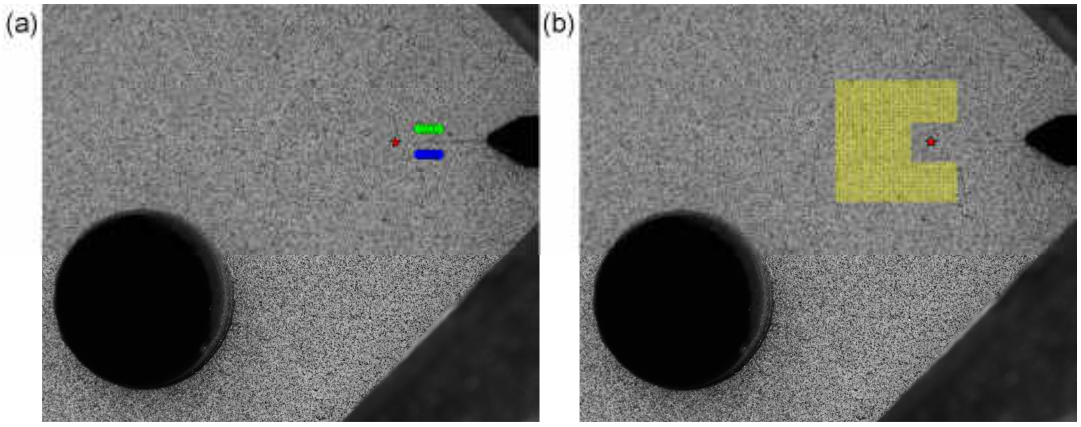

Figure 6. Exemplary data for (a) Symmetrical points used for COD-LSM method (b) Displacement data used for LSM method.

A Matlab routine (Gonzáles et al. 2016) was used to experimentally obtain the SIF values using the afore mentioned methodologies. Figures 7a through 7e present a comparison of SIFs values obtained from COD-LSM and LSM methodologies with the values obtained from Finite Element (FE) simulations performed at total crack lengths of 4.1 mm, 6.3 mm, 8.2 mm, 10.2 mm and 11.9 mm, respectively. Figure 7f presents the location of the crack tip where the SIFs were evaluated. The 3D finite element analysis was performed using the Autodesk Simulation Multiphysics software. All the material properties were input into the FE program assuming an isotropic linear material model. It used about 3 mm tetragonal, and tetrahedral elements in the general body, whereas a refinement was made around the crack tip in a 10 mm radius, with quarter-point elements of approximately 0.37 mm.

Both of the afore mentioned methods (COD-LSM and LSM) show very close behaviors as seen in Figure 7a for a straight crack and in Figures 7b to 7e for a curved crack. Additionally, experimental results are compared with FE simulations. It can be seen in Figure 7a (4.1 mm straight crack) that the K_I values exhibit a nonlinear behavior at low loads which is compatible with crack closure as identified by Elber. For fatigue grown crack at low load ratios (R = 0.1 in this case), crack closure it is expected to appear. This phenomenon causes an offset between the FE simulation and the experimental SIF values. It is clear that the FE simulation assumes the crack is fully opened during the loading cycle, neglecting the non-linear effects induced by crack closure. Moreover, it can be observed that the K_{II} values are zero or near-to-zero, as the crack is straight, and it is far away from the stress concentration region induced by the drilled hole. Similar results are observed in Figure 7b (total crack length of 6.3 mm). As the crack propagates, it grows toward to the hole, curving its path.

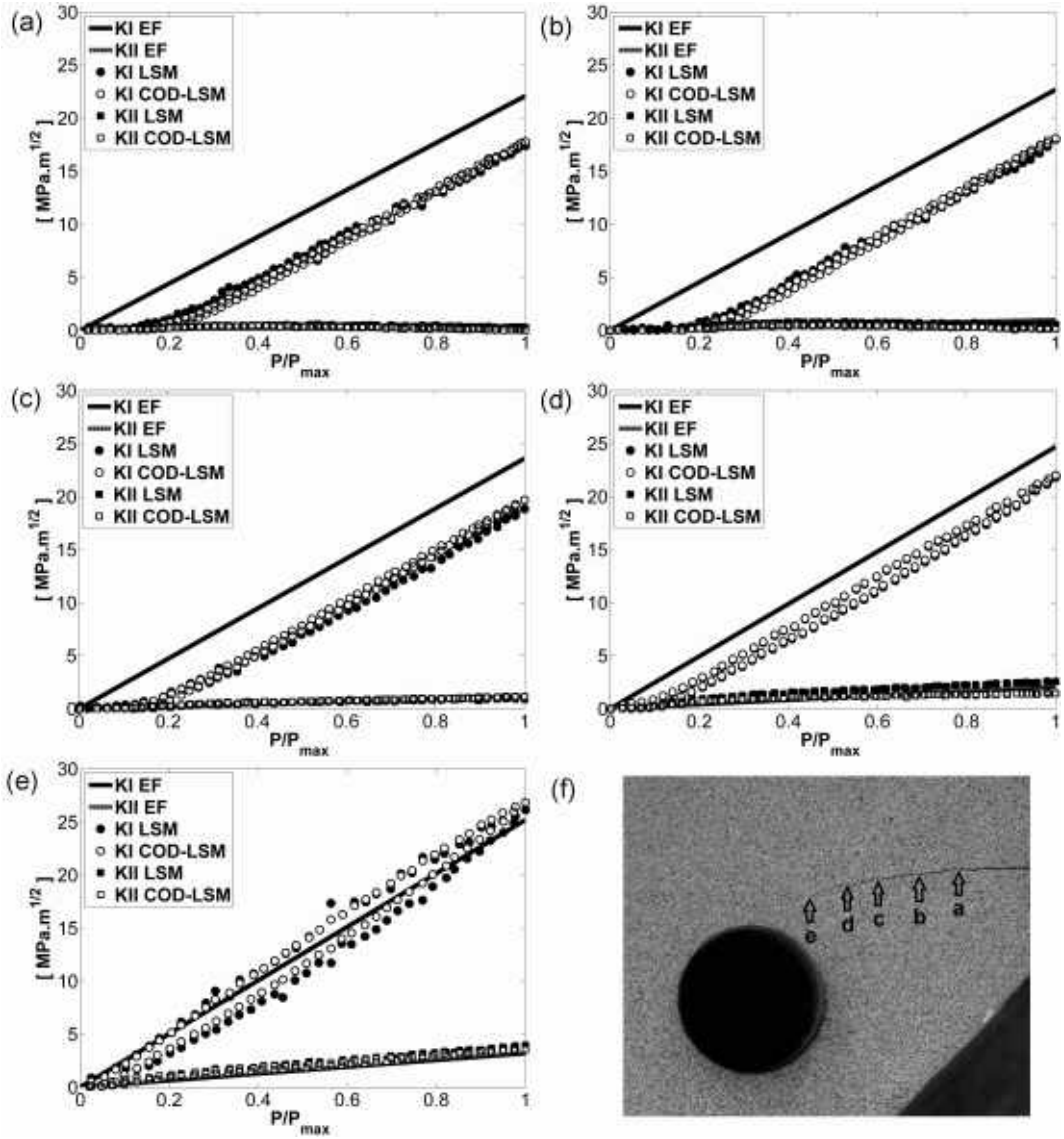

Figure 7. Comparison between experimental and simulated values of SIFs for different crack lengths: a) 4.1, b) 6.3, c) 8.2, d) 10.2 and e) 11.9 mm

In Figure 7e (total crack length of 11.9 mm) the crack has turned at about 24° degrees with respect to the horizontal. In these test conditions, crack closure is not observed in K_I values. Moreover, it is noted that the K_I values (for both experimental methods, COD-LSM and LSM) do not follow the same path during the loading and unloading part of a loading cycle. The fact that the effects of crack closure become less significant as the crack grows toward the hole, curving its path, is an indicator that the crack tip is being significantly affected by the stress concentration field generated by the hole. Thus, it is expected that the strain levels in the surrounding crack tip region will be much higher than the previous measurement points, as can be seen in Figure 5. Finally, Figure 8 shows the evolution of the maximum numerical and experimental K_I and K_{II} along with the angle of curvature of the crack during the test versus crack length *a*.

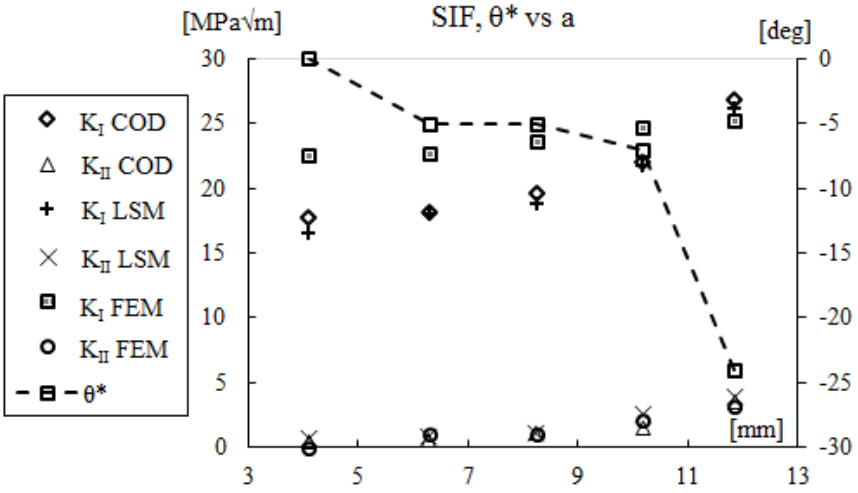

Figure 8. SIF and crack angle versus crack length.

Additionally, Figure 9 depicts the K_{II} values obtained from the COD-LSM method for total crack lengths of 8.2 mm, 10.2 mm and 11.9 mm. It is observed that there is a change of slope in K_{II} values at a load value close to the opening load for the straight crack growing in pure mode I shown in Fig. 7.a (at about 0.27 of P/P_{max}). This behavior is due to the fact that the crack faces partially or completely slip in mode II after or before crack opening in mode I. It is out of the scope to discuss this point in the present paper, and more explanation about this phenomenon can be found in Kibey et. al. (Kibey, Sehitoglu, and Pecknold 2004).

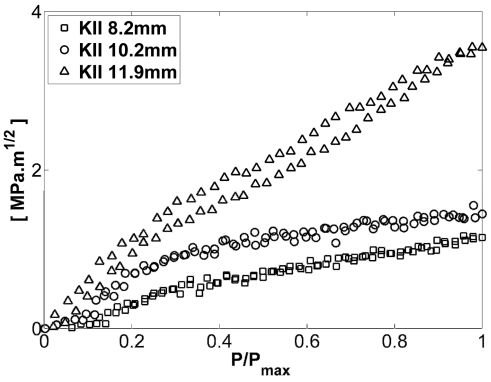

Figure 9. Experimental K_{II} values for different crack lengths.

Table 2 presents the maximum values for SIFs obtained with both experimental methods (COD-LSM and LSM), as well as the maximum SIFs from numerical results, their respective crack length and crack kinking angles (θ*) measured from the horizontal axis for the points illustrated in Figure 7f.

Table 2. Maximum values of experimental SIF for the evaluated points.

Point	a [mm]	θ^*	K_I COD- LSM	K_{II} COD LSM	K_I LSM	K_{II} LSM	K_I FEM	K_{II} FEM
a	4.1	0	17.7	0	16.4	0.4	22.5	0
b	6.3	-5	18.1	0.1	18	0.5	22.7	1
c	8.2	-5	19.7	1.1	18.8	0.9	23.6	1
d	10.2	-7	22	1.4	21.8	2.6	24.7	2.1
e	11.9	-24	26.8	3.5	26.1	4	25.2	3.2

There are many criteria that explain crack path under mixed-mode conditions. Among them are: the Maximum Tangential (Normal) Stress (MTS) criterion which states that a crack under mixed-mode loading will propagate in the direction perpendicular to the maximum tangential (normal) stress and ahead of the crack tip, or the strain energy density (SED) criterion which predicts crack growth along the direction of minimum strain energy density or the Maximum Energy Release Rate Criterion (MERR) which expresses that a crack will propagate in the direction in which the energy release rate is maximum - see (Mróz and Mróz 2010) for a comprehensive review. All of those criteria acknowledge that

crack initiation happens when their particular property attains a critical value. The mentioned criteria are solely based on LEFM and the crack kinking is directly related to K_{II} influence. That is being said, for K_{II} equal to zero, the crack path ought to keep straight. The T-stress (stress parallel to the crack and not reported here) is known to influence brittle fracture when the stress field is result of mode II loading (Smith, D. J. Ayatollahi 2001) or impact crack path steadiness in pure mode I under mixed-mode loading that includes minor imperfections (Kim and Paulino 2003). The evaluation of these criteria, using data acquired from the present experiment, is under analysis and shall be presented in a future publication.

6. CONCLUSION

The paper has shown a consistent and simple methodology to calculate SIFs values under mixed-mode conditions from full field displacement data, in this case obtained via DIC technique. The LSM method fits displacements to evaluate SIF from the coefficients in Williams´ series, whereas the COD-LSM uses the relative displacement between two or more than two opposite-to-crack points. The advantage of the COD-LSM method is that it uses the COD measurements, which has been proven to be certain and simple, but it makes it a more robust measure by including more data points.

Variations in the stress intensity factors K_I and K_{II} were observed as the crack is attracted toward the hole.

It is expected that experimental results represent the real behavior of the tested sample, whereas simulation results represent the sample´s behavior based on a numerical model. Therefore, it can be added that although elastic FE simulations can model crack behavior and can calculate fracture mechanic´s parameters such as SIF, J-integral or the Energy release rate, so far models, which simulations are based on, cannot reproduce non-linear behaviors such as those reported in this paper.

7. ACKNOWLEDGMENT

Gonzales G. L. G. gratefully acknowledges the support of the CNPq (reference 152795/2016-2). In addition, Díaz J. G. and González J. A. O. are thankful for their CAPES/PRO-EX scholarships. Finally, the authors want express their gratitude to Mr. H. Matos Andrade from HCG Equipamentos, São Bernardo SP, for the XRF analysis.

8. REFERENCES

Becker, T. H., M. Mostafavi, R. B. Tait, and T. J. Marrow. 2012. “An Approach to Calculate the J-Integral by Digital Image Correlation Displacement Field Measurement.” *Fatigue and Fracture of Engineering Materials and Structures* 35: 971–84.

Castro, Jaime Tupiassu Pinho, and Marco Antonio Meggiolaro. 2016. *Fatigue Design Techniques, Vol III*. 3rd ed. USA: CreateSpace.

Gonzáles, Giancarlo Luis et al. 2016. “Determining SIF Using DIC Considering Crack Closure and Blunting.” In *Experimental and Applied Mechanics. Vol 4.*, ed. Alan T. Zehnder. Orlando, FL: Springer, 25–36.

Harilal, R., C. P. Vyasarayani, and M. Ramji. 2015. “A Linear Least Squares Approach for Evaluation of Crack Tip Stress Field Parameters Using DIC.” *Optics and Lasers in Engineering* 75: 95–102. http://www.sciencedirect.com/science/article/pii/S0143816615001566.

Ju, S. H., S. H. Liu, and K. W. Liu. 2006. “Measurement of Stress Intensity Factors by Digital Camera.” *International Journal of Solids and Structures* 43(5): 1009–22.

Kibey, S., H Sehitoglu, and D.A. Pecknold. 2004. “Modeling of Fatigue Crack Closure in Inclined and Deflected Cracks.” *International Journal of Fatigue* 129(3): 279–308. https://link.springer.com/article/10.1023/B:FRAC.0000047787.94663.c8.

Kim, Jeong Ho, and Glaucio H. Paulino. 2003. “T-Stress, Mixed-Mode Stress Intensity Factors, and Crack Initiation Angles in Functionally Graded Materials: A Unified Approach Using the Interaction Integral Method.” *Computer Methods in Applied Mechanics and Engineering* 192(11–12): 1463–94.

Lopez-Crespo, P et al. 2008. “The Stress Intensity of Mixed Mode Cracks Determined by Digital Image Correlation.” *The Journal of Strain Analysis for Engineering Design* 43: 769–80.

Mróz, K. P., and Z. Mróz. 2010. “On Crack Path Evolution Rules.” *Engineering Fracture Mechanics* 77(11): 1781–1807.

De Oliveira Miranda, Antonio Carlos, Marco Antonio Meggiolaro, Jaime Tupiassú Pinho De Castro, and Luiz Fernando Martha. 2003. “Fatigue Life Prediction of Complex 2D Components under Mixed-Mode Variable Amplitude Loading.” *International Journal of Fatigue* 25(9–11): 1157–67.

Peters, W. H., and W. F. Ranson. 1982. “Digital Imaging Techniques In Experimental Stress Analysis.” *Opt. Eng.* 21(3).

Peters, W.H. et al. 1983. “Application Of Digital Correlation Methods To Rigid Body Mechanics.” *Opt. Eng.* 22(6).

Réthoré, J., A. Gravouil, F. Morestin, and A. Combescure. 2005. “Estimation of Mixed-Mode Stress Intensity Factors

Using Digital Image Correlation and an Interaction Integral." *International Journal of Fracture* 132(1): 65–79.
Roux, Stéphane, and François Hild. 2006. "Stress Intensity Factor Measurements from Digital Image Correlation: Post-Processing and Integrated Approaches." *International Journal of Fracture* 140(1–4): 141–57. http://link.springer.com/10.1007/s10704-006-6631-2.
Smith, D. J. Ayatollahi, M. R. PavierM. J. 2001. "The Role of T-Stress in Brittle Fracture for Linear Elastic Materials under Mixed-Mode Loading." *Fatigue and Fracture of Engineering Materials and Structures* 24: 137–50.
Sutton, M.A., J. J. Orteu, and H. Schreier. 2009. *Image Correlation for Shape, Motion and Deformation Measurements: Basic Concepts, Theory and Applications*. Boston: Springer.
Sutton, M. A. et al. 1983. "Determination of Displacements Using an Improved Digital Correlation Method." *Image and Vision Computing* 1(3).
Vormwald, Michael et al. 2017. "Variable Mode-Mixity during Fatigue Cycles – Crack Tip Parameters Determined from Displacement Fields Measured by Digital Image Correlation." *Frattura ed Integrita Strutturale* 41: 320–28.
Williams, Max L. 1957. "On the Stress State at the Base of a Stationary Crack." *Journal of Applied Mechanics* 24(march): 109–14.
Yates, J. R., M Zanganeh, D Asquith, and Y H Tai. 2009. "Quantifying Crack Tip Displacement Fields : T- Stress and CTOA." In *Crack Paths 2009*, , 57–74.
Yoneyama, S., S. Arikawa, S. Kusayanagi, and K. Hazumi. 2014. "Evaluating J-Integral from Displacement Fields Measured by Digital Image Correlation." *Strain* 50(2): 147–60.
Yoneyama, S., Y. Morimoto, and M. Takashi. 2006. "Automatic Evaluation of Mixed-Mode Stress Intensity Factors Utilizing Digital Image Correlation." *Strain* 42(1): 21–29.
Zhang, Rui, and Lingfeng He. 2012. "Measurement of Mixed-Mode Stress Intensity Factors Using Digital Image Correlation Method." *Optics and Lasers in Engineering* 50(7): 1001–7. http://dx.doi.org/10.1016/j.optlaseng.2012.01.009.

9. RESPONSIBILITY NOTICE

The authors are the only responsible for the printed material included in this paper.